Invited Paper

System trade-offs in a swept source FMCW LiDAR with dispersive OPA beam steering

Mennatallah Kandil[a,b], Marcus S. Dahlem[b], and Wim Bogaerts[a]

[a]Ghent University - IMEC, Photonics Research Group, Department of Information Technology, Technologiepark-Zwijnaarde 126, 9052 Gent, Belgium
[b]IMEC, Kapeldreef 75, 3001 Leuven, Belgium

ABSTRACT

A solid-state FMCW LiDAR system on a photonic chip can be subdivided into its scanning engine and ranging engine. The scanning engine consists of the laser source and beam steering optics, while the ranging engine consists of a modulated transmitted signal and a coherent receiver. Here, we present the practical considerations of using the wavelength of a swept laser source for both FMCW ranging and beam steering through a dispersive optical phased array (DOPA). Controlling both functions with a single variable (the laser wavelength) is very attractive from a system perspective. The DOPA maps the wavelength injected in its input port to a unique spot in the far-field. Thanks to reciprocity, this mapping also works in reverse and so the reflected beam is sent back to the same input port. Consequently, the DOPA not only provides a simple mechanism for the steering and receiving optics, but also a strong rejection of unwanted signals, since the DOPA acts both as a spatial and a spectral filter. Steering based on sweeping the wavelength can be combined with the frequency ramping for FMCW ranging. The sweep rate and tuning range of the laser determines the far-field coverage, as well as the depth resolution and precision of the ranging engine. The design freedom of the system can be extended by feeding multiple lasers in parallel into the DOPA, without the need for extra wavelength filters. The use of multiple lasers simultaneously (each illuminating different far-field locations), combined with the discretized DOPA architecture, represents a promising approach to system scalability. We analyze the trade-offs and constraints arising in our system, due to the coupling of the parameters of the scanning engine and the ranging engine. In addition, we model the imperfections along the path of the optical signal, starting from its generation by the tunable laser up to its detection on the coherent receiver. The model is then used to analyze the impact of the system parameters on the LiDAR performance metrics.

Keywords: LiDAR, FMCW, OPA

1. INTRODUCTION

Solid state LiDAR is currently a hot research topic supporting various applications. However, it has been driven mainly by the automotive industry.[1] One can sub-divide solid-state scanning LiDAR system into scanning engine (choosing the spatial direction) and ranging engine (measuring the distance). There is vast array of implementation alternatives for the building blocks of both engines with their trade-offs and challenges. Throughout the paper, we will build up the logic of our proposed system to overcome, on the long term, the limitations of current implementations.

The main functionality of LiDAR is to build a 3D point cloud of the environment, where the angular direction is determined from the antenna far-field direction, the depth/distance is determined from the emitted signal delay time, and the radial velocity is determined from Doppler frequency shift of the emitted signal wavelength. The required specifications to construct this point cloud depends on the application, but we will use the approximate specifications for forward-looking automotive LiDAR to direct our discussion about our proposed LiDAR system. These are listed in Table 1.

Further author information: (Send correspondence to M.K.)
M.K.: E-mail: menna.kandil@imec.be

Smart Photonic and Optoelectronic Integrated Circuits 2024, edited by Sailing He, Laurent Vivien, Proc. of SPIE Vol. 12890, 128900I
 · 0277-786X · doi: 10.1117/12.3002492

Horizontal field of view	50	°
Vertical field of view	20	°
Angular sampling resolution	0.1	°
Beam divergence	0.06	°
Center Wavelength	1550	nm
Range	200	m
Range resolution	15	cm
Frame rate	25	Hz

Table 1: Approximate specifications for forward-looking automotive LiDAR.

2. THE SCANNING ENGINE

For the scanning engine, one approach that is particularly interesting, from the point of view of integrated photonics, is based on solid-state optical phased arrays (OPA). Other implementation such as mechanical scanners or MEMs-based scanners can be found in literature[2].[3] In this work, we solely follow the OPA approach.

2.1 OPA implementations

A phased array is an array of antennas in a 1D or 2D configuration, where the phase and amplitude of the feed signal to each antenna determines the far-field profile of the array. In the integrated photonics domain, waveguide gratings can be used as antennas. Upon placing the antennas in a uniform array and feeding each consecutive antenna in the array with a signal of fixed phase increment, one gets a collimated beam spot in the far-field, where the direction of the beam is determined by the phase increment value. Thus, phased arrays offer non-mechanical beam scanning by controlling the phases (and amplitude) of the array input signals. Phased arrays have been well-known in the RF field for a long time,[4] while optical phased arrays (OPAs) with on-chip antennas and on-chip phase control got first demonstrated in integrated photonics through the work of Van Acoleyen *et al.*[5]

The manipulation of the phase (and amplitude) of the feed signal in each antenna has been an active research topic. One way is to add phase shifters (e.g. heaters) before the antennas, whether the antennas are organized in a 1D array[6] or a 2D array.[7] Using calibration algorithms, one can build a look-up table for the state of each of the phase shifters versus the desired far-field profile and direction.[8] Using a 2D array of antennas represents a massive challenge in terms of control, footprint and power consumption, as the number of antennas increases dramatically, and it becomes more complicated to feed the signal into the many antennas.

One way to simplify the phase shifter-based implementation is to use a 1D array of long grating-based antennas fed by a tunable laser,[6] where the phase tuners control the direction of the beam in the horizontal direction. In the vertical direction, the far-field angle of emission of the gratings is controlled by tuning the wavelength of the laser. However, looking practically into automotive LiDAR requirements (Table1), an aperture of $\approx 30\,\text{mm} \times \approx 30\,\text{mm}$ is required to project the beam over Rayleigh range of 200m with farfield divergence of 0.006°. In addition, to scan over a field of view (FoV) of 25° (half of what we actually list in the specs), one needs the antennas to be placed at pitch (d)$\approx 3.47\,\mu\text{m}$ at design center wavelength $\lambda = 1.55\,\mu\text{m}$, where $FoV \approx \arcsin\frac{\lambda}{d}$. This amounts to 8000 - 16000 antennas, and therefore 8000 - 16000 phase tuners are required to achieve LiDAR FoV and spot size requirement. This is still a huge challenge.

There is an option to eliminate the active phase shifters. The use of the tunable laser can be extended to achieve full 2D passive beam steering,[9] where cumulative delay lines are added to the 1D antenna array. Instead of adding phase shifters before each antenna, it is fed with an increasingly long waveguide with fixed increments in delay. Due to the optical path length, the phase difference between antennas becomes a function of the wavelength, as illustrated in Fig. 1. Thus, this continuous dispersive optical phased array (DOPA) maps each wavelength to a different far-field direction.

Despite the simplicity of the continuous DOPA implementation, it comes with multiple challenges in terms of footprint, insertion loss, and phase errors introduced mainly due to the distribution network.[11]

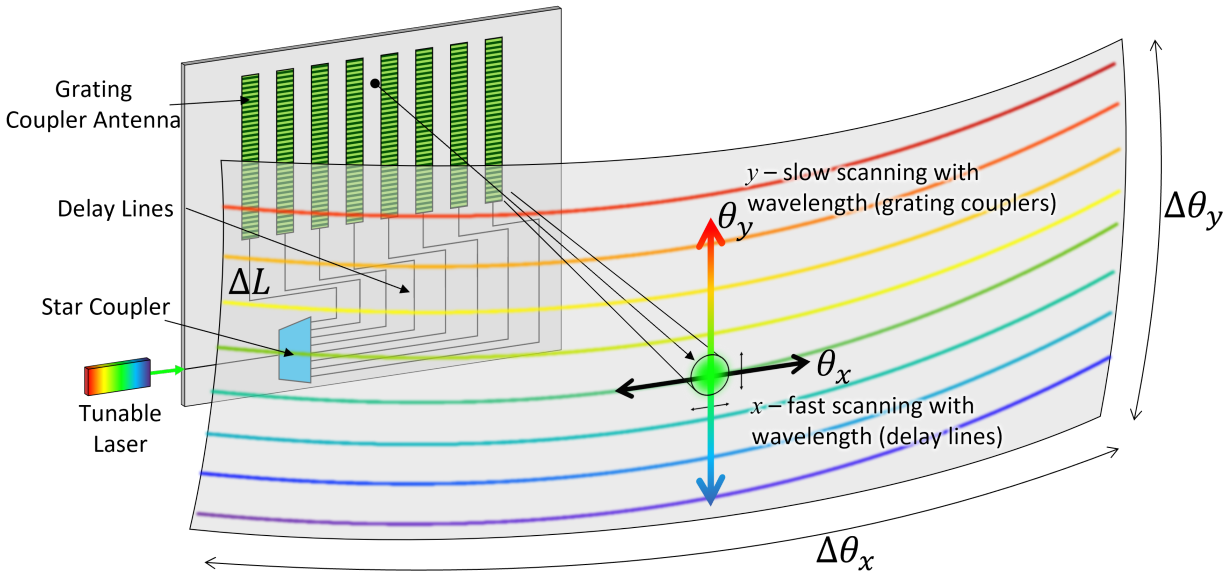

Figure 1: Beam steering with a continuous DOPA. The tunable laser sweeping achieves 2D beam steering. Along the fast axis, the farfield beam angle follows the laser wavelength due to the waveguide dispersion of the delay lines, while along the slow axis, the farfield beam angle follows the laser wavelength due to the gratings dispersion. Figure adapted from.[10]

2.2 Pixellated (discretized) dispersive OPA with a swept source

Upon close investigation, we can see that the emitting aperture needs to fulfill the area and fill factor requirements to achieve the FoV and far-field divergence requirements. However, there are degrees of freedom in the distribution network design itself. One of these degrees of freedom crystallizes by separating the far-field spot size requirement from the far-field angular resolution requirement. The LiDAR range requirement for the DOPA imposes certain size for the array in order to have acceptable beam divergence at the maximum range. On the other hand, this narrow far-field spot gives us a far-field sampling angle resolution that is far larger than the angular resolution requirement or the number of far-field pixels we want to collect. By keeping the aperture the same as continuous DOPA, but subdividing the distribution network into smaller blocks, we can decouple the spot size requirement of the range and the resolution of the farfield sampling.

What do we mean by subdividing the distribution network? The principle was first introduced in the the work of Bogaerts *et al.*[11] Let's take an example of an antenna array of W elements. Instead of a distribution network where the first delay line is of length ΔL and the last delay line is of length $W.\Delta L$, we will subdivide the distribution network into M identical blocks. Each block feeds N antennas, where $W = M.N$. The first delay line in the block is of length ΔL and the last delay line is of length $N.\Delta L$. The blocks can be fed by any 1×M splitter such as a balanced splitter tree or a star coupler, as shown in Fig. 2.

What would be the effective behavior of such distribution network? As the wavelength is swept, within each block, the phase relation between each two consecutive antennas is the same as in the continuous DOPA, however, that incremental phase relation between the antennas of different blocks is broken. Since all the blocks are fed by a $1 \times M$ splitter, the phase at the input of all the blocks is the same, regardless of the wavelength. Effectively, specific wavelengths will achieve constructive interference leading to narrow beam in the far-field, and for those wavelengths the full discretized DOPA gives the same field profile as the continuous DOPA.[10] However, between those particular wavelengths, the phase delay between the blocks is not matching the phase delay within the blocks, and there is not single focused beam. The result is that the continuous scan lines now become pixellated. For example, consider a DOPA with the design parameters from Table 2. Choosing to split it into 64 blocks gives ≈ 8000 pixels in the far-field over the wavelength tuning range, and the total insertion loss

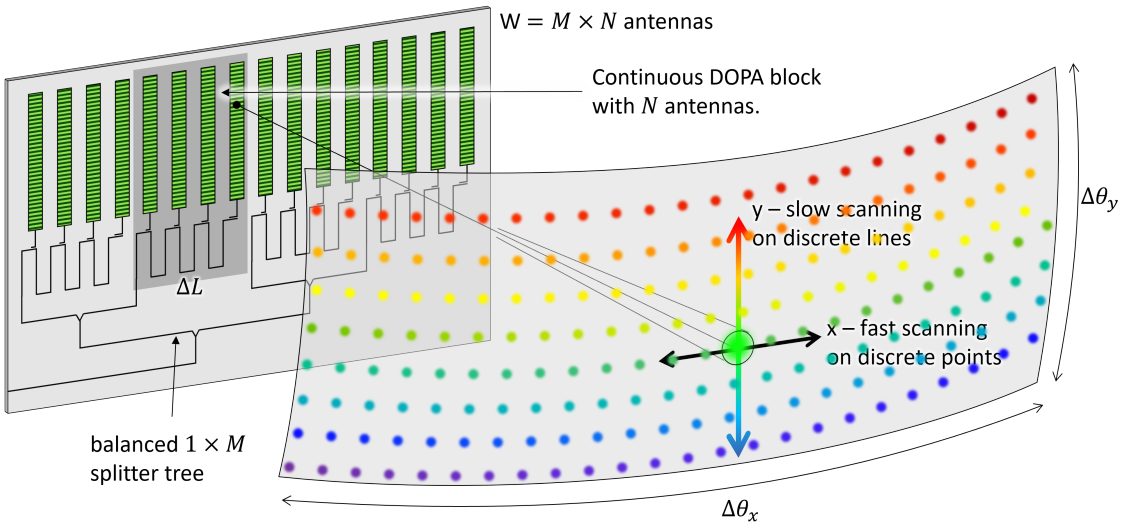

Figure 2: Beam steering with a pixelated DOPA. The emitting aperture is the same as in the continuous DOPA, but the distribution network is subdivided into smaller blocks. The distribution network of each block is snake-like. It is also possible to use an unbalanced splitter tree or AWG-like distribution network for each block. All the blocks are fed by a balanced splitter tree. Figure adapted from.[10]

Center wavelength	1550	nm
Wavelength tuning range	100	nm
Total number of antennas	8192	
Array pitch	3.47	µm
Delay line length	634	µm
Waveguide loss	0.2	dB/cm
Waveguide effective index	2.4	
Waveguide group index	4.5	

Table 2: Example of the design parameters of the DOPA.

of the distribution network is ≈ 0.81 dB, as shown in Fig. 3. Consequently, the number of blocks determines the far-field sampling and the distribution network insertion loss.

This is why we call this implementation a pixelated DOPA, as one gets farfield pixels instead of farfield scan lines when sweeping the tunable laser. With good design choices, the discretized DOPA allows scaling to large number of antennas and provides a room for further degrees of freedom for the system design, as will be discussed in Section 4.

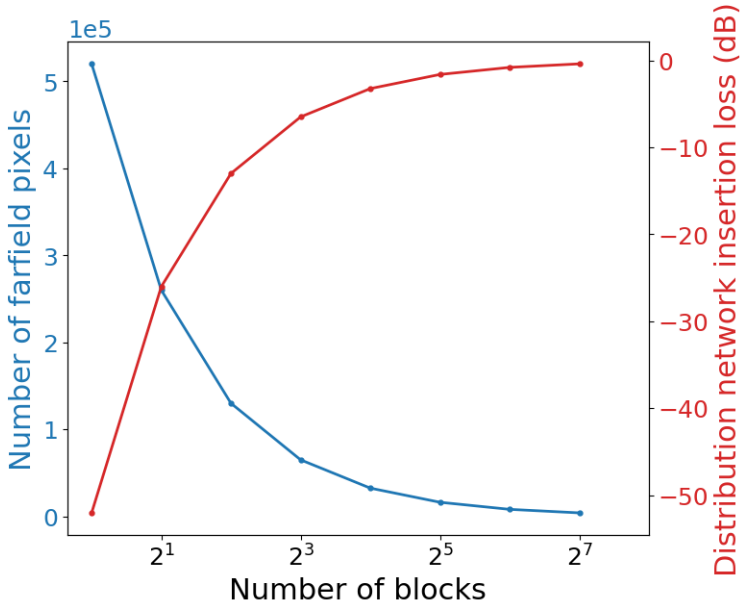

Figure 3: Effect of the number of blocks on the number of farfield pixels and on the delay lines distribution network insertion loss for the unbalanced splitter tree architecture.

3. THE RANGING ENGINE

Coherent detection has been a practical receiver solution for various optical communication systems in both optical fibers[12] and free space communication[13] to improve receiver sensitivity and to reduce signals cross-talk. A LiDAR link is in essence a high loss communication channel, which makes coherent detection schemes a natural choice. The frequency modulated continuous wave (FMCW) scheme is one of the most popular implementations of coherent detection for LiDAR.[1]

3.1 FMCW ranging

3.1.1 FMCW ranging working principle

In an FMCW receiver, a sawtooth (or triangular for velocity detection) frequency waveform (FMCW chirped signal), is generated directly from the laser by sweeping the laser emission wavelength. The chirp rate of the frequency waveform is:

$$\gamma = \frac{\Delta f_{sweep}}{T_{sweep}}, \tag{1}$$

where f_{sweep} is the chirp (sweep) bandwidth and T_{sweep} is the chirp (sweep) time.

The laser signal is split into 2 signals: a local oscillator signal E_{LO} which goes into the coherent receiver input, and the beam scanning signal which is emitted in free space and bounces back into the receiver from the target as a return signal E_{RX} after time delay of Δt_{TOF}, as pictured in Fig. 4. The return signal E_{RX} is collected by the receiving optics, then goes into the coherent receiver input where it gets mixed with the local oscillator signal. The instantaneous frequency of the output baseband signal is the beat frequency f_{beat}, where the range is calculated as follows:

$$R = \frac{c.\Delta t_{TOF}}{2} = \frac{c.f_{beat}}{2\gamma}. \tag{2}$$

As we show in Fig. 5, the range is estimated using a digital signal processor (DSP) to identify the peak frequency in the beat signal's discrete Fourier transform. The nature of the operation of coherent detection makes it a strong candidate for solid-state automotive LiDAR. One of its main advantages is its immunity to ambient light, since in order to mix the return signal with the local oscillator signal, they need to be coherent; which means that

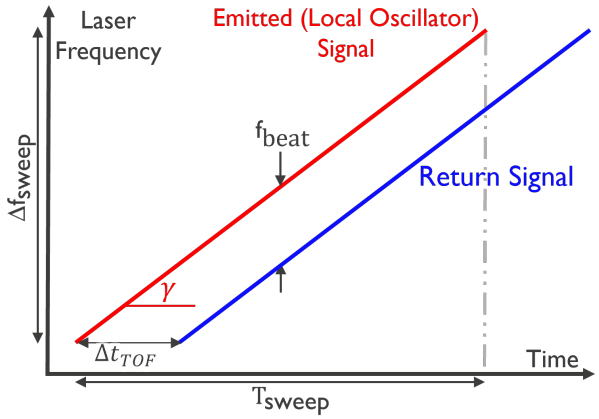

Figure 4: FMCW signal.

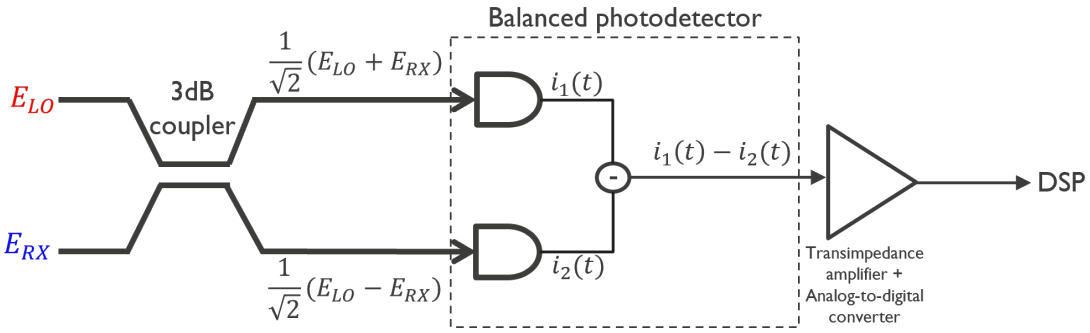

Figure 5: FMCW coherent detector.

cross-talk from other light sources is largely filtered out. Furthermore, the LiDAR return signal is normally very weak, but in a coherent shot-noise limited detector, it gets amplified by mixing it with the local oscillator signal, enabling the detection of these very weak signals. In addition, the beat signal frequency is the down-converted return signal frequency (by local oscillator) which can be electronically processed.

3.1.2 Ranging key performance metrics

The main performance metrics associated with ranging performance are the range resolution δR and range precision σ_R.

Range resolution: δR is the minimum distinguishable (resolvable) axial distance between closely spaced targets. Two targets spaced by more than δR will be individually resolved in range; targets spaced by less than δR will not. δR is fundamentally limited by the chirp bandwidth:[1]

$$\delta R = \frac{c}{2BW} = \frac{c}{2\Delta f_{sweep}} \tag{3}$$

Range precision: The goal of LiDAR ranging measurement is to estimate the range from the received signal, and the standard deviation of the range estimate error is the range precision. Following information theory, the Cramer-Rao (CR) lower bound establishes the minimum achievable variance of the range estimator. It has been shown that the range precision follows:[1]

$$\sigma_R \geq \frac{c}{2BW\sqrt{SNR}} = \frac{\delta R}{\sqrt{SNR}} \tag{4}$$

Equations 3 and 4 show that the sweep bandwidth and the signal-to-noise-ratio (SNR) of the system are the fundamental limiting factors for the ranging engine.

3.1.3 Signal-to-noise ratio

Understanding the foundations of SNR in coherent detection permits us to clearly identify some of the design challenges of our photonic system. What is the signal in the SNR? In our work, we use the electrical current generated in the detector. What is the noise? There are many sources of noise, but for an initial estimation, we consider the thermal noise and the shot noise in the analog domain. Can we set a requirement for the SNR? Taking range precision equation (eq.4) into consideration, the SNR requirement can not be decreased indefinitely at the expense of increasing the sweep bandwidth to satisfy the precision requirement. There is a lower bound for the SNR[14] ($SNR_{threshold}$) that can be determined by the desired detection probability and the probability of false alarm. A typical starting value for such a design is SNR of 13.2 dB for detection probability of 0.9 and probability of false alarm of 10^{-6}.[15]

SNR of a coherent detector can be derived as follows, assuming the noise spectrum is that of white noise:

$$SNR = \frac{Signal\ spectral\ density}{Noise\ spectral\ density} = \frac{Coherent\ signal\ power\ spectral\ density}{Noise\ power\ spectral\ density\ .\ BW_{measurement}}$$

Since we integrate over the measurement time in FMCW LiDAR: $BW_{measurement} = \frac{1}{T_{meas}}$

$$SNR = \frac{S^2_{coherent}}{\sigma^2_{Thermal} + \sigma^2_{shot}}.T_{meas} = \frac{R^2_{PD}P_{RX}P_{LO}}{\frac{4KT}{R} + 2qR_{PD}P_{LO}}.T_{meas}$$

The SNR can be improved by increasing the local oscillator power up to a certain limit where the shot noise dominates the thermal noise. In the shot noise limited regime, which can be considered the mode of operation for FMCW, the SNR becomes:

$$SNR = \frac{R_{PD}P_{RX}}{2q}.T_{meas} \tag{5}$$

where R_{PD} is the photodetector responsivity [A/W], P_{RX} is the optical power in the receiver collected from the target reflection, P_{LO} is the optical power from the local oscillator in the coherent receiver, q is the electron charge.

This means that, in terms of system design, we have a main trade-off between the measurement time and receiver power to achieve the required SNR.

For a measurement time that is set by design (for example based on frame rate requirement), the minimum power on the detector (i.e. receiver sensitivity) can be calculated:

$$P_{RX} \geq \frac{2q}{R_{PD}}.\frac{1}{T_{meas}}.SNR_{threshold} \tag{6}$$

3.2 FMCW ranging with a swept source

In our proposed system, the tunable laser's full capability can be leveraged by controlling both the beam scanning and ranging functions with a single wavelength variable.[16] In such system, the design parameters of the scanning and ranging engines are partially coupled, which provides new degrees of freedom for design, but also comes with new design challenges and trade-offs. Throughout the upcoming sections, we will present the considerations for the design of such system.

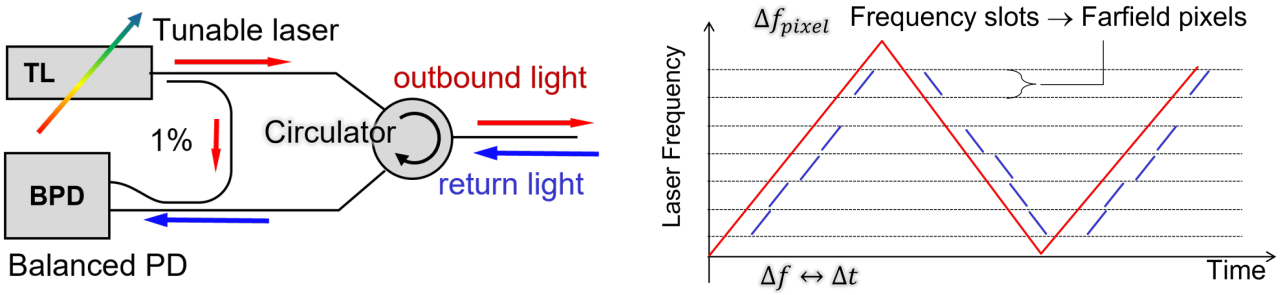

(a) Ranging engine (b) Frequency slots.

Figure 6: FMCW ranging engine with swept source.

3.2.1 Frequency slots in ranging and farfield pixels in scanning

Let's consider a typical wavelength (frequency) sweep that is used for DOPA beam scanning from 1500 nm to 1600 nm. For the pixelated DOPA, such sweep includes a certain number of pixels, depending on the choice of the number of blocks M. From the FMCW ranging perspective, considering a ≈ 1 GHz chirp bandwidth, such sweep can include up to ≈ 12486 frequency slots (detection data points). Combining both perspectives, each farfield pixel should correspond to an FMCW chirp frequency slot: the sweep bandwidth within the slot corresponds to the angular pixel size in the far field. This shows an example of the coupling between the scanning engine requirements(angular resolution) and the ranging engine requirements(range resolution). In this implementation, the coherent detector is constantly detecting the received signal throughout the full sweep time, but in the processing stage, the signal will then be divided into frequency slots on which a rolling FFT is performed, as shown in Fig. 6(b). This system alleviates some of the restrictions on the conventional implementation of FMCW LiDAR. Firstly, there is no need for the scanning engine to wait for the return signal to move to the next pixel, which gives extra freedom in the choice of the system time parameters. In addition, it is possible to have multiple return signals on the receiver that are detectable and distinguishable (in terms of range and direction), which falls under the multiple tone frequency estimation problem.[14]

3.2.2 Coupling between the angular resolution and range resolution requirements

Let's consider three consecutive wavelengths that fulfill the constructive interference condition of the pixellated DOPA (corresponding to three spatially adjacent farfield pixels) for the OPA in Table 2, with $N_{blocks} = 64$ blocks. The array factor at these wavelengths shows a side lobe suppression ratio (SLSR) $> 13dB$ for uniform feed power distribution over the antennas, as shown in Fig. 7(a).

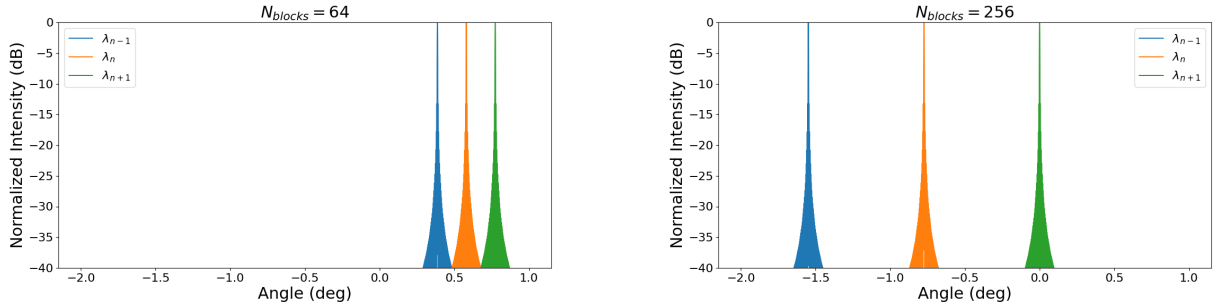

(a) (b)

Figure 7: The array factor of three consecutive constructive wavelengths in pixellated DOPA representing three adjacent pixels, for different number of blocks.

We consider the wavelength (frequency) sweep around the wavelength λ_n in Fig. 7(a). To achieve a range resolution of 15 cm, the sweep bandwidth needs to be 1 GHz which corresponds to ≈ 7.6 pm wavelength range

around λ_n, eq. 3. To assess the pixellated DOPA performance within this wavelength range, we inspect the SLSR. At these wavelengths, prominent side lobes are observed at the angles of the neighbouring pixels (due to the diffraction orders of the OPA constructed from the blocks), as can be seen in figure 8(a) where there is prominent peaks at the angles of the neighbouring pixels. The SLSR is degrading far below 13 dB and the pixellated DOPA performance degrades from the corresponding continuous DOPA, as can be seen from Fig. 9(a). When we reduce Δf_{sweep} to 0.5 GHz, which corresponds to $\approx$ 3.3 pm range around the center wavelength and results in range resolution of 30 cm, an SLSR $>$ 13 dB can be achieved, as can be seen from Fig. 9(a). When increasing the number of blocks to 256, we reduce the number of farfield pixels and increase the angular resolution as shown in Fig. 7(b), and then we observe an SLSR $>$ 13 dB within the wavelength range corresponding to range resolution of 15 cm, as shown in Fig. 9(b).

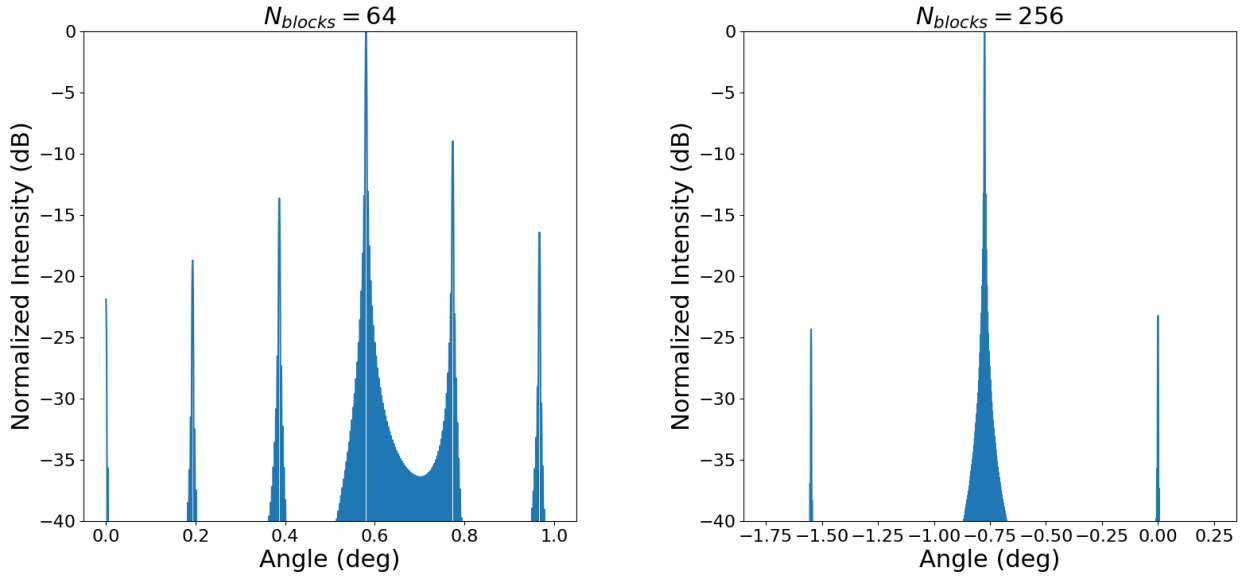

(a) (b)

Figure 8: The array factor of at wavelength of λ_n - 3 pm, for different number of blocks.

This means that in the pixellated DOPA, the full bandwidth between pixels can not be fully used for some sets of design choices due to the sharp decrease of the SLSR, and hence of the SNR, which is shown in Fig. 10. To sum up, a good design approach to dealing with such trade-off would take into account: choosing number of blocks that avoids the collapse of SLSR within a frequency slot while maintaining an acceptable insertion loss of the circuit, and choosing acceptable range resolution without violating the angular pixel size requirement[17] to avoid pixels aliasing.

3.3 Receiver sensitivity and LiDAR equation

In a LiDAR engine, the losses along the optical signal path from its generation by the laser up to detection is modelled by the LiDAR/RADAR equation. Assuming a monostatic configuration for the transmitter and receiver circuit, and the target object model being diffuse Lambertian surface scatterer, the LiDAR equation can be written as:[18]

$$P_{RX} = P_T \eta_p \rho(\pi) \frac{\pi D^2}{4z^2} \tag{7}$$

where P_{RX} is the power at detector, P_T is the power fed to the transmitter circuit, η_p is efficiency factor that includes the insertion loss of the optical circuit, emission/receive efficiency, atmospheric losses, and heterodyne efficiency (equals 100% in integrated photonics), $\rho(\pi)$ is the inverse steradian power reflectivity of the target, D is the diameter of receive aperture, and z is the distance to the target.

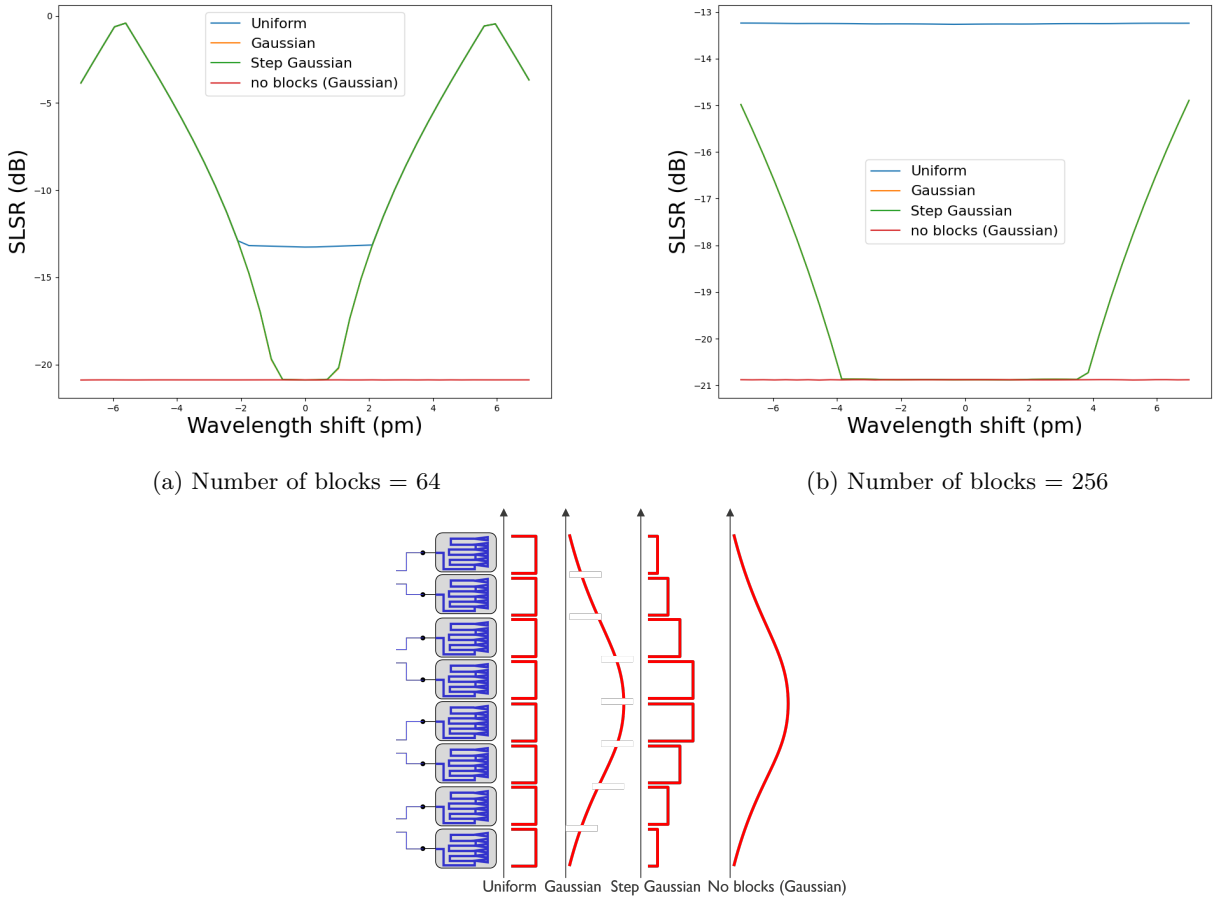

(a) Number of blocks = 64

(b) Number of blocks = 256

Figure 9: SLSR at different wavelength shifts from λ_n, for different number of blocks.

Equations 6 and 7 show that for a certain transmitter/receiver design and a certain measurement time, the maximum range is limited by the receiver sensitivity to achieve $SNR_{threshold}$. For example, consider a system with measurement time set to 20 µs and the photodetector responsivity is $0.8A/W$, this sets the receiver sensitivity to 0.4179 pW, according to eq. 6. In terms of transmitter/receiver design, we take the radiation/receive efficiency as 9.8 %, the receive aperture size is ≈ 30 mm. As we use a monostatic configuration, we can start the LiDAR equation from the emitted power from transmitter and still be able to anaylze the effect of circuit design. In this particular analysis, it is better to start from emitter power rather than laser power so we can set the emitted power to the eye safety limit (10 dBm) regardless of the transmitter circuit loss. Assuming no atmospheric losses and the target reflectivity in the direction of the receiver circuit is 20 %, the maximum range is limited to ≈ 90 m for distribution network loss of 15 dB, shown in Fig. 11. By only improving the distribution network loss with good choices for discretization (Fig. 3), one can push the maximum range to to 300 m (Fig. 11).

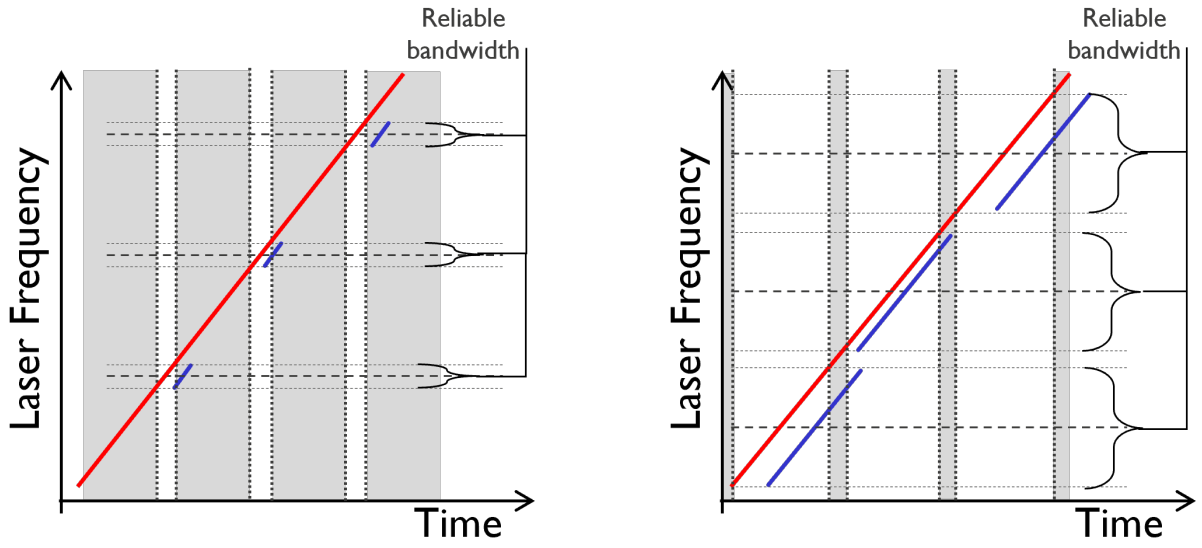

(a) Number of blocks = 64 (b) Number of blocks = 256

Figure 10: Three adjacent pixels represented by the frequency sweep, where the bandwidth between the pixels can not be fully used due to low SLSR of the pixellated DOPA at these frequencies (not to scale). Increasing the number of blocks, increases the angular resolution and gives acceptable SLSR within the bandwidth corresponding to range resolution of 15 cm.

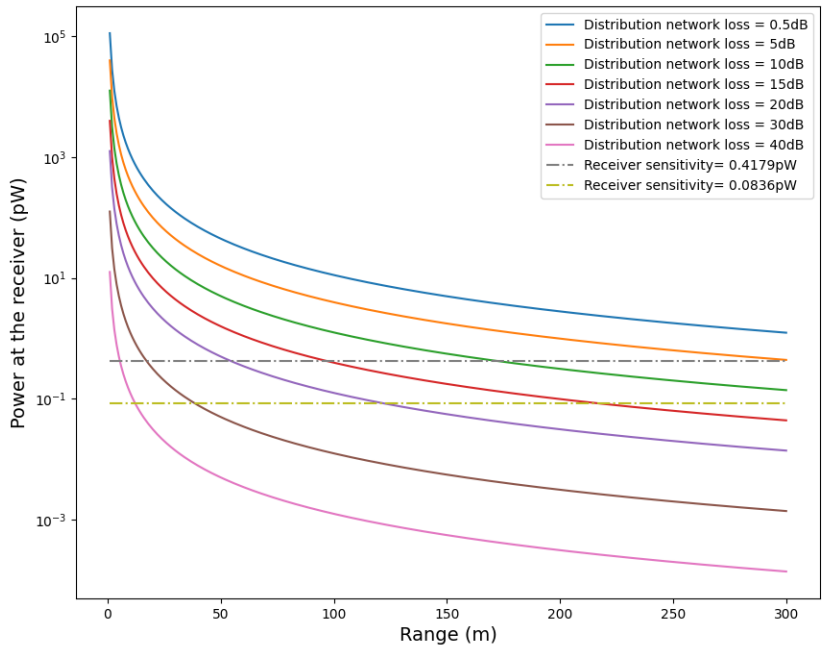

Figure 11: Power at the receiver versus range for different values of distribution network loss, and receiver sensitivity for measurement duration of $20\mu s$ and $100\mu s$.

4. ACHIEVING FRAME RATE SPECIFICATION: MULTIPLEXING

In a pixellated DOPA, a star coupler can be used to distribute light to the blocks, as mentioned in section 2.2. Instead of a star coupler with a single input aperture, multiple input apertures on a Rowland circle can be used to achieve wavelength multiplexing. Each aperture is connected to a separate FMCW ranging engine, where each engine has a tunable laser covering a band that is subsection of the full wavelength tuning range, as illustrated in Fig. 12. In addition, spatial multiplexing can be combined with wavelength multiplexing, where tunable lasers with overlapping wavelength bands are used and the input apertures of the star coupler are positioned in such a way that they cover the full farfield. This multiplexing scheme allows addressing multiple pixels simultaneously, which allows longer measurement duration per pixel within the desired frame rate. Longer measurement time allows the relaxation of the required receiver sensitivity to achieve $SNR_{threshold}$. Let's take an example of a system that targets to scan 100000 pixels with a frame rate of 25 Hz (40 ms per frame). One can use 32 lasers, where the mode-hop-free bandwidth of each laser is 400 GHz, and use a spatial multiplexing factor of 8. This gives measurement time per pixel of $\approx 100\,\mu s$.

Linking back to receiver sensitivity and continuing on the example of section 3.3, for the same system except for the measurement time set to 100 µs instead of 20 µs, the receiver sensitivity becomes 0.0836 pW. Consequently, we can see in Fig. 11 that the maximum range, for distribution network loss of 15 dB, is pushed from ≈ 90 m to ≈ 200 m.

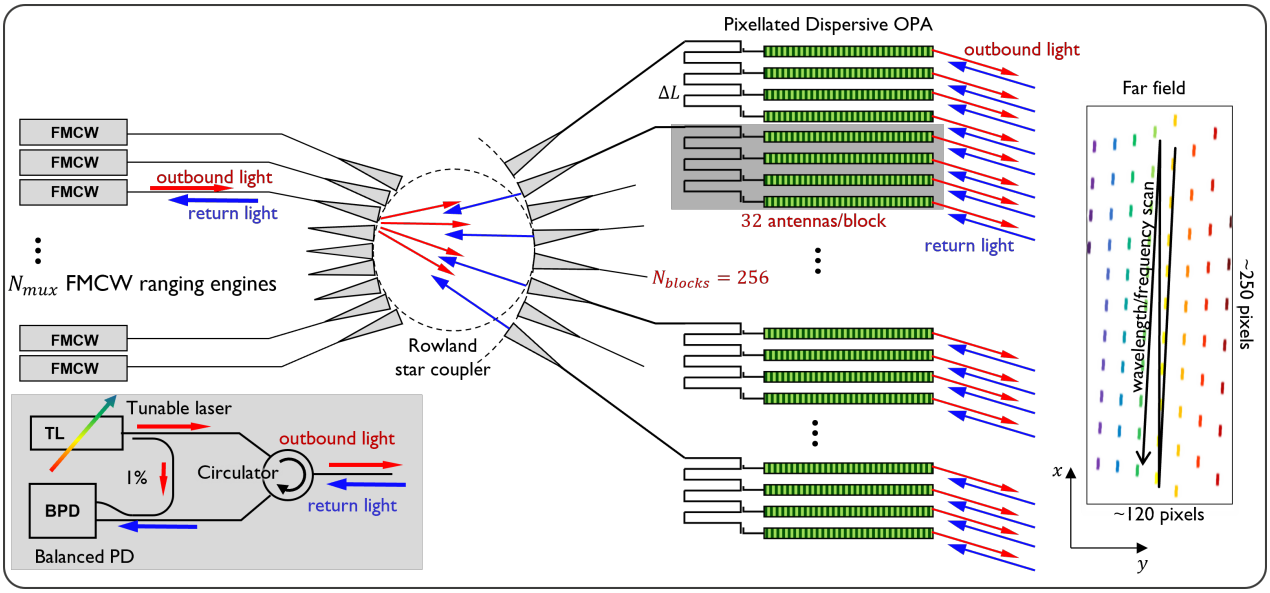

Figure 12: Multiplexed 2D pixellated DOPA beam scanner with FMCW ranging engines. A swept source is used to achieve both beam scanning and LiDAR ranging. Multiple FMCW engines are connected to the star coupler input ports to address multiple farfield pixels simultaneously.

5. CONCLUSION

We presented the implications of pixellated DOPA design choices for the scanning engine on the ranging engine performance in a system that uses a single wavelength variable to achieve both beam scanning and ranging for automotive LiDAR. We illustrated the effect of discretization on the number of farfield pixels and circuit insertion loss. We discussed the considerations to deal with the trade-off between the angular resolution requirement of scanning engine and the range resolution requirement of the ranging engine. In addition, we discussed the trade-off between the range, circuit losses and ranging integration time to achieve the SNR required for reliable detection. Finally, we presented a multiplexing scheme that allows having enough integration time for reliable detection while achieving the desired frame rate for automotive LiDAR.

REFERENCES

[1] Behroozpour, B., Sandborn, P. A. M., Wu, M. C., and Boser, B. E., "Lidar system architectures and circuits," *IEEE Communications Magazine* **55**(10), 135–142 (2017).

[2] Roriz, R., Cabral, J., and Gomes, T., "Automotive lidar technology: A survey," *IEEE Transactions on Intelligent Transportation Systems* **23**(7), 6282–6297 (2022).

[3] Royo, S. and Ballesta-Garcia, M., "An overview of lidar imaging systems for autonomous vehicles," *Applied Sciences* **9**(19) (2019).

[4] Stark, L., "Microwave theory of phased-array antennas—a review," *Proceedings of the IEEE* **62**(12), 1661–1701 (1974).

[5] Acoleyen, K. V., Bogaerts, W., Jágerská, J., Thomas, N. L., Houdré, R., and Baets, R., "Off-chip beam steering with a one-dimensional optical phased array on silicon-on-insulator," *Opt. Lett.* **34**, 1477–1479 (May 2009).

[6] Acoleyen, K. V., Rogier, H., and Baets, R., "Two-dimensional optical phased array antenna on silicon-on-insulator," *Opt. Express* **18**, 13655–13660 (Jun 2010).

[7] Sun, J., Timurdogan, E., Yaacobi, A., Hosseini, E. S., and Watts, M. R., "Large-scale nanophotonic phased array," *Nature* **493**, 195–199 (Jan 2013).

[8] Kjellman, J. Ø., Prost, M., Marinins, A., Tyagi, H. K., Kongnyuy, T. D., Kerman, S., Troia, B., Figeys, B., Dwivedi, S., Dahlem, M. S., Soussan, P., Rottenberg, X., and Jansen, R., "Silicon photonic phase interrogators for on-chip calibration of optical phased arrays," in [*Integrated Optics: Devices, Materials, and Technologies XXIV*], García-Blanco, S. M. and Cheben, P., eds., **11283**, 112830X, International Society for Optics and Photonics, SPIE (2020).

[9] Van Acoleyen, K., Bogaerts, W., and Baets, R., "Two-dimensional dispersive off-chip beam scanner fabricated on silicon-on-insulator," *IEEE Photonics Technology Letters* **23**(17), 1270–1272 (2011).

[10] Bogaerts, W., Dwivedi, S., Jansen, R., Rottenberg, X., and Dahlem, M. S., "A 2d pixelated optical beam scanner controlled by the laser wavelength," *IEEE Journal of Selected Topics in Quantum Electronics* **27**(1), 1–12 (2021).

[11] Bogaerts, W., Dahlem, M., Dwivedi, S., Jansen, R., and Rottenberg, X., "Dispersive optical phased array circuit for high-resolution pixelated 2D far-field scanning controlled by a single wavelength variable," in [*Smart Photonic and Optoelectronic Integrated Circuits XXII*], He, S. and Vivien, L., eds., **11284**, 112841Z, International Society for Optics and Photonics, SPIE (2020).

[12] Ip, E., Lau, A. P. T., Barros, D. J. F., and Kahn, J. M., "Coherent detection in optical fiber systems," *Opt. Express* **16**, 753–791 (Jan 2008).

[13] Chan, V. W. S., "Free-space optical communications," *Journal of Lightwave Technology* **24**(12), 4750–4762 (2006).

[14] Rife, D. and Boorstyn, R., "Single tone parameter estimation from discrete-time observations," *IEEE Transactions on Information Theory* **20**(5), 591–598 (1974).

[15] Skolnik, M., [*Introduction to Radar Systems*], Electrical engineering series, McGraw-Hill (2001).

[16] Bogaerts, W., Kandil, M., and Dahlem, M. S., "Integrated optical beam scanning and fmcw ranging using multiplexed tunable lasers," in [*2022 IEEE Photonics Conference (IPC)*], 1–2 (2022).

[17] Okano, M. and Chong, C., "Swept source lidar: simultaneous fmcw ranging and nonmechanical beam steering with a wideband swept source," *Opt. Express* **28**, 23898–23915 (Aug 2020).

[18] Osche, G. R., [*Optical Detection Theory for Laser Applications*] (2002).